Formation of thermal plumes in an autocatalytic exothermic chemical reaction

Bice S. Martincigh,[1] Marcus J. B. Hauser,[2] and Reuben H. Simoyi[3]
[1]*Department of Chemistry and Applied Chemistry, University of Natal, Private Bag X10, Dalbridge 4014, Republic of South Africa*
[2]*Institut fur Physikalische Chemie, Universitat Wurzburg, Marcusstrasse 9-11, 97070 Wurzburg, Germany**
[3]*Center for Nonlinear Science and the Department of Chemistry, West Virginia University, Box 6045, Morgantown, West Virginia 26506-6045*
(Received 29 June 1995)

The reaction of chlorite and thiourea is bistable and displays a lateral instability that generates a traveling wave of sulfate, acid, and chlorine dioxide. The wave was visualized by the addition of barium chloride, which gave a white precipitate of barium sulfate. The wave propagates with three distinct regions of varying precipitation intensities. One of the regions is made up of a complete convective roll that forms powerful thermal plumes which rise to the surface of the reactant solution. The plumes originate from a coupling of Marangoni convection with multicomponent convection.

PACS number(s): 47.70.Fw, 47.20.Dr, 82.20.Mj

INTRODUCTION

The existence of dissymmetry and chirality seem to be the fundamental properties upon which life and living systems thrive [1,2]. Spatiotemporal organization, as well, seems to be heavily involved in the sustenance of life. The stripes on a zebra and the spots on a leopard are just some of the examples of spatiotemporal organization in living systems [3]. In an epoch-making paper in 1952, mathematician Alan Turing suggested that structures similar to these biological examples could be replicated in chemical systems due to the coupling of chemical reaction and diffusion [4]. Turing's paper sparked a lot of activity from theoreticians, biologists, and chemists, all trying to generate Turing-type stationary patterns from unstirred chemical reaction solutions. If indeed Turing patterns could be generated from structureless media, then it might be possible to rationalize morphogenesis in which an embryo develops from an erstwhile structureless medium [5]. It is generally understood that different steady states (inhomogeneous, periodic, and chaotic), that have lower symmetry than appropriate equations and boundary conditions, emerge at bifurcation points that mark qualitative changes in the dynamic behavior of the system [6].

State equations involved in most chemical, hydrodynamic, and biological systems are symmetric with respect to time, space, rotations, and inversions [7]. The existence of symmetry simplifies the task of solving state equations, as one should obtain solutions with the same symmetry as the problem. Nonlinear problems, however, may possess more than one solution (e.g., patterns), and asymmetric solutions may be the only ones stable enough with respect to small perturbations, especially if the symmetric solutions are subject to excitability [8].

Pattern formation can easily be explained in reaction-diffusion systems by invoking two or more coexisting mechanisms with different characteristic time or length scales [9]. One mechanism will destabilize the symmetric state, and another will simultaneously prevent the unlimited growth of perturbations. A typical example is the mechanism of local activation with lateral diffusion, in which we combine a rapidly diffusing inhibitor with a slowly diffusing activator [10]. With $\mathbf{U}_1$ as the activator and $\mathbf{U}_2$ as the inhibitor, the following reaction-diffusion equations for the one dimensional case can be generated:

$$\delta_t U_1 = D_1 \delta_x^2 U_1 + a_1 U_1 - b_1 U_2 \tag{1}$$

and

$$\delta_t U_2 = D_2 \delta_x^2 U_2 - a_2 U_2 + b_2 U_1 \ , \tag{2}$$

where D_1, and D_2 are the diffusion coefficients, b_1 and b_2 are the cross-coupling terms, and a_1 and a_2 are the growth rates.

Solutions of Eqs. (1) and (2) give a chemical wavelength q_0 of

$$q_0 = \tfrac{1}{2}[a_1/D_1 - a_2/D_2]^{1/2} \ . \tag{3}$$

From the diffusion coefficient and growth rate, one can define a decay length (or range) l_i as

$$l_i = \sqrt{(D_i/a_i)} \ .$$

For patterns to develop, D_1 and D_2 must be sufficiently different such that

$$l_1^{-2} - l_2^{-2} > 0 \ . \tag{4}$$

Patterns will then spontaneously develop with wavelength q_0. Thus when the major reactive species have vastly differing diffusion coefficients, one can expect symmetry-breaking bifurcations in chemical systems even at isothermal conditions.

Spatiotemporal patterns have been observed in many nonequilibrium fluid systems such as the Rayleigh-Bérnard convection [11] and Taylor-Couette flow [12].

*Present address.

In many dissipative systems spatially periodic structures develop out of a homogeneous state when the driving force exceeds a critical value [13]. In the Rayleigh-Bénard instability a critical bifurcation parameter could be the temperature difference between the two plates [14]. Convection and buoyancy have been adequate in describing most spatiotemporal pattern formation and traveling wave generation in fluids heated from below and closed to the atmosphere [15].

A full description of such patterns in systems, which can include lateral heating [16] and fluids with a freely deformable upper surface, requires the addition of thermocapillary convection [17]. Patterns generated from very thin horizontal fluid layers can effectively be described by invoking the Marangoni effect only, and neglecting thermogravitational effects [18].

Attempts are now underway to study systems that combine both reaction-diffusion and convective mechanisms, DCR (diffusion-convection reaction) [19]. Typical systems that can be studied are highly exothermic bistable (or excitable) chemical reaction systems [20]. In the absence of temperature control, heat then becomes an additional parameter in determining the stability of the chemical reaction system [21]. Already, recent studies have found lateral instabilities in DCR systems which are not supported by the accepted theory for isothermal reaction-diffusion systems [22]. For example, in isothermal systems, quadratic autocatalysis is insufficient to effect a lateral instability (at least cubic autocatalysis is required) [23], while in DCR systems lateral instabilities have been observed with quadratic autocatalysis [22].

In this paper we want to report on the very fascinating observation of thermal plumes or volcanic-type eruptions we have observed in the wake of a traveling wave generated in the exothermic reaction of chlorite and thiourea in neutral to slightly acidic environments. While rapid traveling waves have been observed in exothermic bistable chemical reaction systems, we believe this is the first time such powerful yet coherent eruptions have been observed in very dilute thin layer reaction solutions.

Chemical properties of the wave

The reaction being studied in the oxidation of a thiocarbonyl compound, thiourea, by chlorite [24]. The oxidation products are sulfate and urea:

$$(NH_2)_2C{=}S+2ClO_2^-+H_2O \rightarrow SO_4^{2-}+(NH_2)_2C{=}O+2H^++2Cl^- \ . \quad (5)$$

This reaction presents clock reaction characteristics in which initially there is a quiescent period with no activity in the reaction indicators. At the end of the induction period there is a rapid and sudden production of SO_4^{2-}, ClO_2, and H^+. The acid and SO_4^{2-} are formed simultaneously from the oxidation of the sulfonic acid intermediate [25]:

$$NH_2(NH)CSO_3H+2H_2O \rightarrow SO_4^{2-}+(NH_2)_2C{=}O+4H^++2e^- \ . \quad (6)$$

The ClO_2 is formed by an extraneous ClO_2-HOCl reaction which occurs when ClO_2^- is in stoichiometric excess over thiourea [26]:

$$2ClO_2^-+HOCl+H^+ \rightarrow 2ClO_2+Cl^-+H_2O \ . \quad (7)$$

HOCl is the autocatalytic species which controls the rates of reaction and wave propagation [27,28]. The full mechanism for this reaction has been reported elsewhere [24,25].

Concurrently with the production of H^+, SO_4^{2-}, and ClO_2 is the important production of heat from the enthalpy of the reaction. The heat generated is so high that the reaction of thiourea and chlorite has an enthalpy of reaction of approximately -1160 kJ mol^{-1} [20]. This can give a temperature jump of up to 70 °C at the wave front. In our study the temperature jump was in the range of 3.8–7 °C depending on the initial concentrations used. In unbuffered solutions the productions of H^+ can be used as an indicator for the position of the wave front. Other indicators used include aqueous $BaCl_2$ and freshly prepared starch. The experimental results reported here were performed with $BaCl_2$ as the indicator. Formation of SO_4^{2-} anywhere in the solution will be indicated by the formation of white $BaSO_4$ [29]. The light reflected on the $BaSO_4$ crystals can clearly indicate the direction of fluid flow at the surface and within the bulk of the solution.

EXPERIMENT

Stock solutions were prepared from the following reagents: thiourea (Fisher), sodium chlorite (Kodak), and barium chloride (Caledon Laboratories). The commercially available technical grade sodium chlorite varied in purity from 78 to 81% [30]. The sodium chlorite was recrystallized from a water/ethanol mixture and standardized iodometrically [31]. No other reagents required purification. The stock solutions were prepared fresh daily. Extra care was also given to the chlorite, which was stored in dark winchester bottles to avoid excessive exposure to light.

Reaction mixtures were prepared from these stock solutions to give a final thiourea concentration of 0.020 M, with the sodium chlorite concentration being maintained at (at least) twice the thiourea concentration to ensure the formation of exotic dynamics [18,20]. Barium chloride concentrations were kept at about 0.05 M. Thiourea and barium chloride were vigorously mixed in a beaker, and the sodium chlorite was added last by means of a rapid delivery pipette. After complete mixing, the reaction solution was poured into the reaction vessel, allowed to settle, and then triggered.

The reactions were performed in two large plexiglass vessels. Previous studies had shown that the propagation of the big wave was extremely sensitive to vessel geometry [18]. One vessel was a rectangle of length 24.3 cm and width 15.3 cm. The other vessel was an isosceles triangle of base 16.0 cm and a peak angle of 38°.

Image analysis and wave dynamics

Video imaging experiments were useful for studying the wave velocities, the structure of the propagating wave front, and the spatiotemporal patterns. All experiments were recorded using a PULNIX TMC 74 color camera attached to a Sony PVM-1334Q RGB monitor and a Panasonic AG-1960 professional videocassette recorder. The videocassette recorded and the RGB monitor were also interfaced to a 486-type 33-MHz computer via a PCVision Plus frame grabber model PFGPlus-640-3-60 capable of storing a 640×480 pixel image. Image analysis was via Bioscan OPTIMAS version 4.02 software. The recorded experiments were played back on the videocassette and the desired frames captured and stored as tagged image file format (TIFF) files. The velocities were measured using the motion analysis macro of the Bioscan software, which uses Microsoft Excel 4.0 for the statistical analysis. Further processing of the acquired images included noise and color filtering.

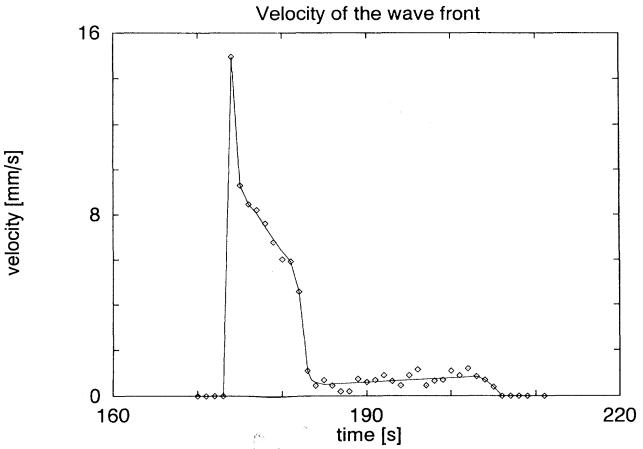

FIG. 1. Wave velocity variation for a self-initiated wave in the chlorite-thiourea reaction. Wave initiates after an induction time of 173 s. Structured precipitation patterns which align themselves along the direction of wave propagation are obtained up to 182 s when the wave finally attains a constant velocity. Thermal planes and volcanic eruptions mentioned in this paper are observed after 182 s. $[NaClO_2]_0=0.045$ M $[SC(NH_2)_2]_0=0.0225$ M, and $[BaCl_2]_0=0.0488$ M.

RESULTS

By using a large vessel, wave observations could be made in the center of the vessel without interference from vessel boundary effects. The chemical waves generated and reported here were all triggered by addition of a drop (about 0.025 mL) of a dilute solution of the autocatalyst HOCl after a time lag of 60 s after mixing the solutions. The time lag allowed the solution to settle and for all the physical ripples across the surface of the solution to die away. Reaction solutions were either triggered from the side of the vessel and allowed to propagate inward or were triggered at the center of the vessel and allowed to propagate outward. The vessels were filled to a depth of 1.7 mm. A depth of 1.7 mm was the lowest depth possible at which the solution surface was flat and uniform. At depth below 1.7 mm the reaction solution could not uniformly wet the plexiglass surface.

The wave could easily be followed by the formation of white barium sulfate precipitate. The wave started very rapidly with a fast lateral velocity. This velocity was not maintained as the wave quickly decelerated to attain some constant velocity which was determined by the initial reactant concentrations [32]. The wave was faster in concentrated solutions and proportionally slower as the dilution was increased. The wave velocity variations with respect to time are shown in Fig. 1. Most of our observations for this paper were made in the region where the wave velocity was constant.

The fluid motion is evident from the movement of the barium sulfate crystals and the spatiotemporal precipitation patterns. Initially, due to the rapid radial flow, the precipitation patterns are aligned radially, as can be seen in Fig. 2(a). At the wave front there is a thin precipitation ring followed by an annulus of no precipitation and the inhomogeneous precipitation patterns [18,33]. Behind the patterns is an area of homogeneous precipitation. By normal diffusion and Brownian motion, the inhomogeneous patterns, with time, gave a uniform homogeneous pattern.

As the wave front's lateral velocity decreases the inhomogeneous patterns are slowly annihilated, as shown in Figs. 2(b) and 2(c). After complete annihilation of the precipitation patterns and attainment of a constant velocity, the wave then displays three distinct precipitation regions [Figs. 3(a) and 3(b)]. After the wave front ring there is a wide region of very faint precipitation (region I). Behind this, is a region of slightly thicker precipitation, (region II), and finally a region of thick homogeneous precipitation (region III).

The most interesting part of this wave and the subject of this paper is that regions II and III are separated by a line of violent hydrodynamic activity in the form of volcaniclike eruptions. Figure 3(a) shows the appearance of all the three regions, and Fig. 3(b) is a schematic sketch of the regions shown in Fig. 3(a). These regions are also divided by the fluid flow. The fluid at the top of region II flows in the direction of wave propagation, while in region III it flows in the opposite direction. This is as a direct result of the discharges from the volcaniclike plumes (thermal plumes). Formation of plumes is also periodic. After being formed between regions II and III; they are next formed along the line dividing regions I and II. The wave front by then will have moved on, and the ring of plumes becomes the region II and III interface. This sequence is repeated indefinitely for as long as the vessel boundaries do not come into play. In large vessels one can observe 10–15 such sequences. The period between thermal plumes is about 7 s. Figure 4 shows a schematic diagram of the repeating plume formation.

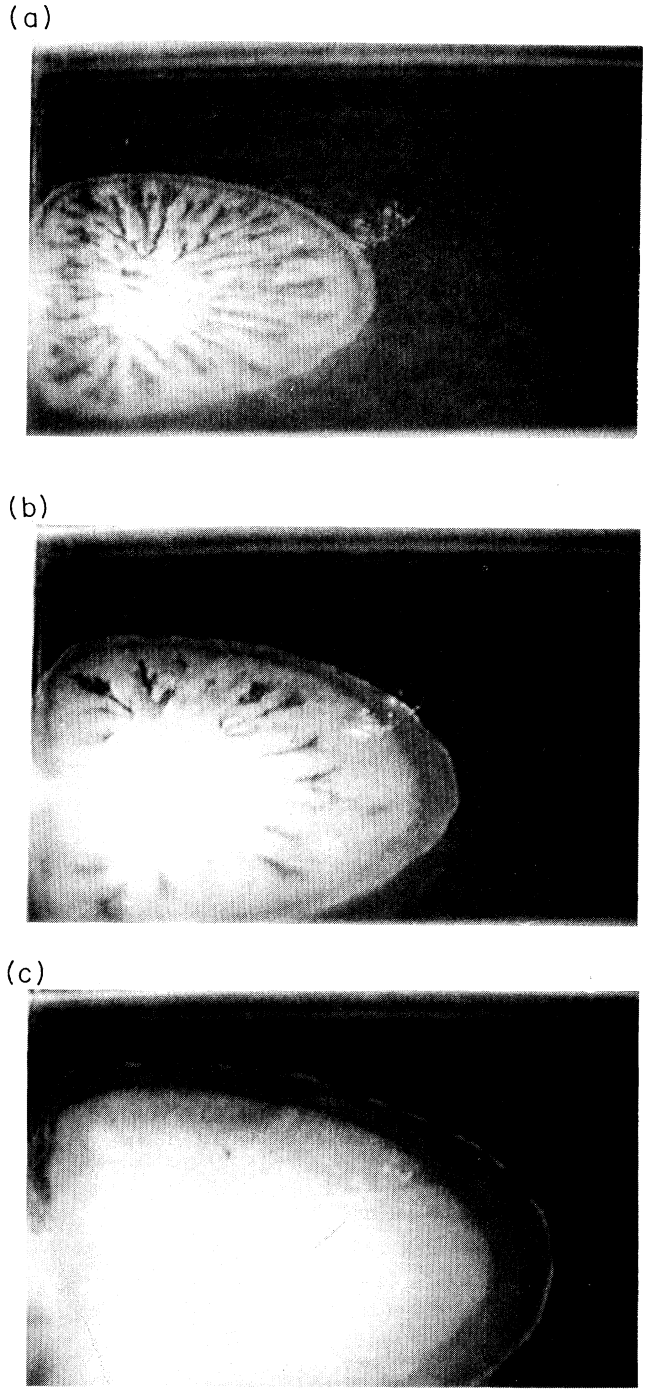

FIG. 2. Structured (or inhomogeneous) precipitation patterns mentioned in Fig. 1. The thin annulus of null precipitation at the edge of the wave front is also quite evident. $[NaClO_2]_0=0.048$ M, $[SC(NH_2)_2]_0=0.024$ M, and $[BaCl_2]_0=0.020$ M. (b) Further development of the wave shown in (a). The inhomogeneous precipitations patterns are beginning to be annihilated, and two regions can now be seen, with the region of faint precipitation at the wave front. (c) Same wave as in (a) and (b) about 5 s after (b). The precipitation patterns have now been destroyed, and three regions can now be seen: faint precipitation (region I), thicker precipitation (region II), and thickest precipitation (region III).

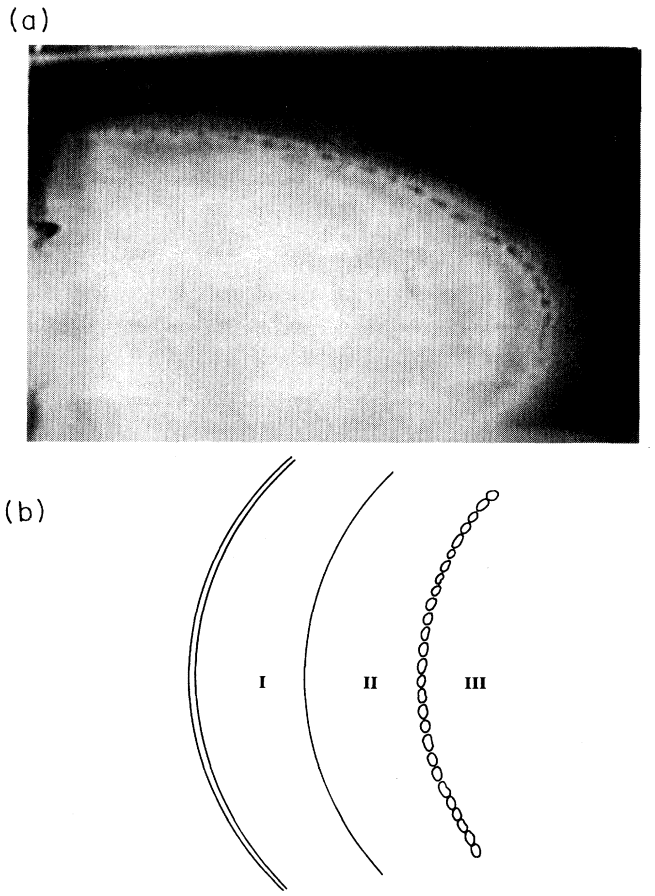

FIG. 3. (a) A picture showing the three regions as well as the thermal plumes at the interface between regions II and III. Experimental conditions are the same as in Fig. 2. (b) A schematic sketch of the picture shown in (a).

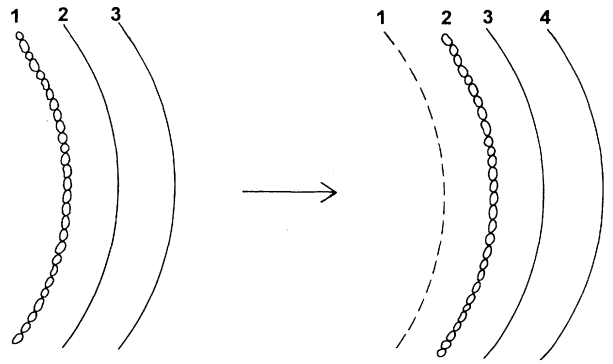

FIG. 4. Repetitive nature of plume formation. Plumes are formed at the interfaces of the different regions. The first sketch shows a normal propagation front with the three interfaces (labeled 1, 2, and 3). Further propagation of the wave forms an interface 4, which is now an additional wave front. Additional plume formation will now occur at interface 2. The position of interface 1 (now part of the bulk homogeneous precipitation region) is denoted by the dashed line.

DISCUSSION

The fascinating behavior being reported here arises from a coupling of reaction, diffusion, thermocapillary effects, and buoyancy. The reaction used for these studies is known to induce multicomponent convection in rising or descending wave fronts [34,35]. This is possible if a negative reaction molar enthalpy is coupled with a negative reaction partial molar volume change [36,37]. If we consider a descending wave front as shown in Fig. 5(a), we can examine the state of the interface between the reacted and unreacted solutions. At isothermal conditions the top reacted solution is heavier than the unreacted solution ($\Delta\rho = -2.7\times10^{-3}$ g cm^{-3}). With the top layer at a temperature 3.8–7 °C higher than the lower solution, the top layer will be temporarily lighter than the unreacted solution until thermal equilibrium is attained [38].

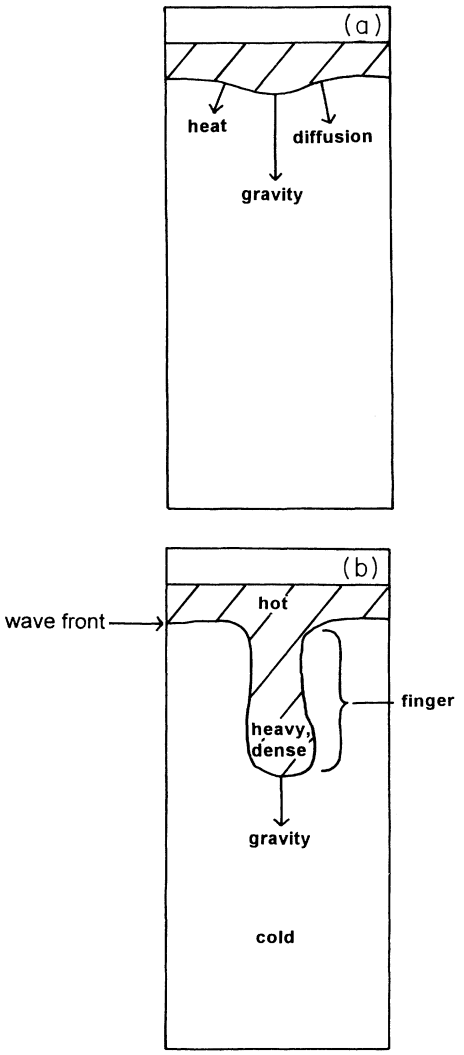

FIG. 5. (a) The mechanism of the formation of a finger. A small deformity at the wave front will continue to grow as it loses heat (and shrinks) much more rapidly than it loses reactants due to diffusion. (b) The shrinkage of the deformity increases its density to where it surpasses that of the reactant solution. Gravitational forces will then pull the reacted solution all the way down into the reactant solution, forming a "finger."

If we assume a Newtonian and incompressible fluid, then the density of the solution is given by [39]

$$\rho=\rho_0[1-\alpha(T-T_0)] , \tag{8}$$

where ρ is the density at temperature, T and ρ_0 is the density at a reference temperature T_0. α is the coefficient of thermal volume expansion [40]. Equation (8) can be set up for both reactants and products. In our system, however, Eq. (8) is of relevance only to the product solution. Double-diffusive convection arises when the following conditions are met:

$$\rho_P(T)<\rho_R(T_0) , \tag{9}$$

but

$$\rho_P(T_0)>\rho_R(T), \quad T-T_0\approx3.8\,^\circ\text{C} , \tag{10}$$

where $\rho_P(T)$ is the density of the product solution at temperature T, and $\rho_R(T_0)$ is the density of the reactant solution at reference temperature T_0. The situation $\rho_P(T)<\rho_R(T_0)$ will predominate until thermal equilibrium is attained. In thin tubes, this situation of a buoyant upper solution can be maintained indefinitely even if the reacted solution is losing heat rapidly [41]. An unstable front will exist in wide tubes as well as in our laterally unbound system.

What happens to a slight deformation of the front, such as is shown in Fig. 5(a)? Heat dissipation is 100 times more efficient than chemical diffusion, so a small deformity protruding into the unreacted region will lose heat rapidly and attain thermal equilibrium with the unreacted region. At isothermal conditions the descending layer is heavier than the bottom layer. Thus the solution in the deformation will start to sink down the unreacted region, forming a salt finger [42] of reacted solution going down the tube as shown in Fig. 5(b). Such an interplay of heat and material exchange exists continuously in the traveling wave front. This interplay will affect mainly the vertical axis motions. A temperature jump in the region of 3–7 °C appears to be ideal for the generation of multicomponent convection. A higher jump will render the top layer permanently lighter than the bottom unreacted region, and no fingering will be observed.

In general, the Rayleigh number [43]

$$\mathrm{Ra}=\alpha g\Delta T d^3\nu\kappa \tag{11}$$

will determine the strength of this buoyancy. In Eq. (11), α is the coefficient of thermal expansion, g is the acceleration of gravity, ν is the kinetic viscosity, κ is the thermal diffusivity, and d is the depth of the solution. This force is heavily dependent on the temperature jump ΔT and the depth of the solution.

The temperature change along the free upper surface introduces a surface tension variation [44]

$$\sigma(T)=\sigma_0-\gamma(T-T_0) , \tag{12}$$

where $\sigma(T)$ is the surface tension at temperature T, and

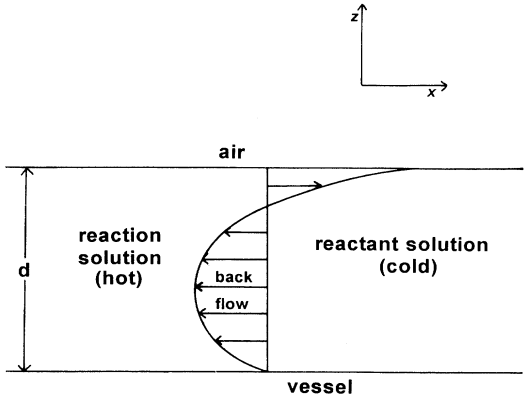

FIG. 6. Diagram of the model used to study the later instability. The maximum forward lateral velocity is at the surface of the wave. From the "nonslip adherence" boundary condition, the return velocity is zero at the bottom of the vessel.

σ_0 is a reference surface tension at T_0. γ is the rate of change of surface tension with temperature. This is usually negative for most fluids, giving a net driving force from hot to cold regions. A negative value for γ for our chemical system means reaction-diffusion forces propagate in the same direction as thermocapillary (Marangoni) effects. A schematic diagram of the effect of thermocapillary effects in the absence of buoyancy effects on a shallow fluid layer is shown in Fig. 6. The surface tension gradient on the free surface will induce a top layer flow which has to be materially balanced by a concomitant return flow at the bottom of the fluid. The shape of the flow curve in Fig. 6 can easily be deduced [43]:

$$v_x = d(d - \tfrac{2}{3}), \quad 0 \le d \le 1 , \tag{13}$$

where v_x is the horizontal velocity and d is the normalized solution depth.

Thermocapillary effects are quantified by the Marangoni number, Ma:

$$\mathrm{Ma} = \gamma \Delta T l / \mu \kappa , \tag{14}$$

where l is the length of the free surface and μ is the dynamic viscosity [45].

Coupling of forces

Significant coupling exists if all three forces (buoyancy, Marangoni convection, and reaction diffusion) are of about the same magnitude. Thus with narrow long tubes the Marangoni effect vanishes as $l \to 0$ and coupling exists only between buoyancy and reaction-diffusion forces. The same applies for very shallow layers ($d \le 1.7$ mm) where the Rayleigh number vanishes as $d \to 0$, and one observes only a thermocapillary effect [18].

The thermal plumes are formed by a convective roll which is formed within the course of wave propagation. The successive sketches of Fig. 7 show how this convective roll is developed. Figure 7(a) shows the basic flow structure as in Fig. 6. The arrow is inserted at the end of the wave to aid the reader. Figure 7(b) shows the start of the formation of a finger. This is formed when the wave has slowed down enough to attain its constant velocity (see Fig. 1). The formation of the finger, as described earlier, is heavily favored by the favorable buoyancy forces as heat is drained from the finger. Figure 7(c) shows the further development of the finger down the solution, and its inevitable turn in the direction opposite the wave

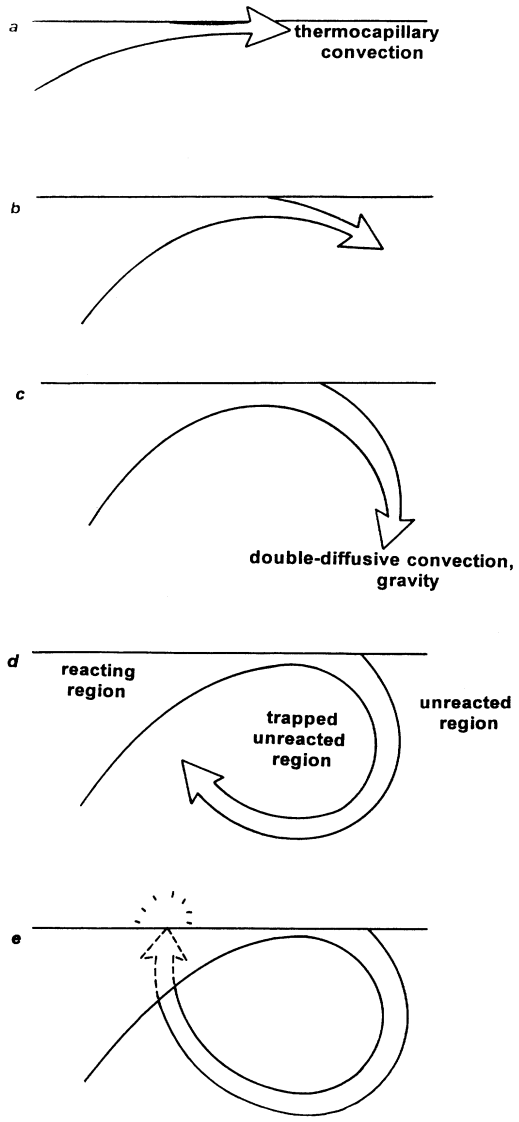

FIG. 7. The development of a convective torus which then forms the thermal plumes. (a) Wave direction during the region of inhomogeneous precipitation. (b) The start of double-diffusive convection as the wave slows down. (c) Pronounced double-diffusive effect coupled with back flow. At this point, apart from gravitational effects, the finger will experience the return flow as seen in Fig. 6. (d) A nearly completed convective roll. (e) A complete convective roll (which is in the form of a torus) which shows the formation of thermal plumes (volcanoes).

propagation. This is due to the back flow, that exists below the surface whose origin is primarily for mass balance. Figure 7(d) shows the completed convective roll as it comes back to meet the original wave, but behind the wave front. Figure 7(d) also shows that the plumes are formed by the collision of fluids flowing in opposite directions; hence the violent eruptions observed. In Fig. 7(e) we attempt to show how the reaction is enhanced at the point of plume formation. As the plume rises through the reacting-reacted region (dashed lines), the reaction is greatly enhanced by the higher temperature within the reacting-reacted region by basic Arrhenius kinetics. Figure 8 is a combination of Figs. 3(b) and 7(e). Here we take a horizontal cross section of Fig. 3(b) and superimpose it on Fig. 7(e) to indicate the three different regions clearly. Faint precipitation in region I is mainly because the wave only occupies the top part of the solution. The inhomogeneity in precipitation in region II is due to the reacting solution moving in different directions (top part moving forward, and the bottom part moving backward).

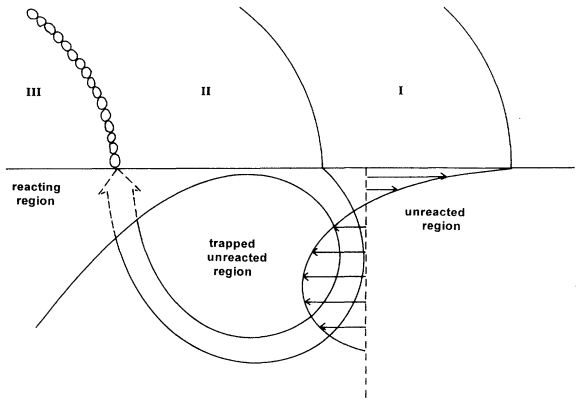

FIG. 8. Combination of Figs. 3(b) and 7(e) which shows the positions of the relevant interfaces.

Role of reaction-diffusion forces in plume formation

So far we have adequately explained the formation of a plume without reference to reaction-diffusion forces. On the time scale of our observations, with wave velocities in the regions of $1-10$ mm s^{-1}, we find diffusive forces insignificant for the description of this phenomenon. The wave propagation velocity is, however, determined by the reaction kinetics. The dominant driving force, convection, is induced by heat (for both buoyancy and Marangoni effects), and the heat is generated by the release of the reaction's free energy (enthalpy change). The critical slowing down of the wave (see Fig. 1) is directly related to the reaction kinetics being unable to sustain the thermocapillary effect from the heat generated.

ACKNOWLEDGMENTS

We thank University of Natal for giving BSM a sabbatical leave. This work was supported by a West Virginia NSF-EPSCoR grant.

[1] R. A. Hegstrom and D. K. Kondepudi, Sci. Am. **262**, 108 (1990).
[2] G. Nicolis, T. Erneux, and M. Herschkowitz-Kaufman, Adv. Chem. Phys. **88**, 263 (1978).
[3] P. Ortoleva and J. Ross, Biophys. Chem. **1**, 87 (1973).
[4] A. M. Turing, Philos. Trans. R. Soc. London Ser. B **37**, 237 (1952).
[5] G. Nicolis and I. Prigongine, *Self-Organization in Nonequilibrium Systems* (Wiley, New York, 1977).
[6] L. M. Pismen, in *Dynamics of Nonlinear Systems,* edited by V. Hlavacek (Gordon and Breach, New York, 1986), pp. 47–84.
[7] M. C. Cross and P. C. Hohenberg, Rev. Mod. Phys. **65**, 851 (1993).
[8] J. J. Tyson and P. C. Fife, J. Chem. Phys. **73**, 2224 (1980).
[9] J. D. Murray, *Mathematical Biology,* 2nd ed. (Springer-Verlag, Berlin, 1983), Vol. 19.
[10] P. Gray and S. K. Scott, *Chemical Oscillations and Instabilities–Nonlinear Chemical Kinetics* (Oxford University Press, London, 1990).
[11] D. Villers and J. K. Platten, Physicochem. Hydrodyn. **8**, 173 (1987).
[12] J. Elezgaray and A. Arneodo, J. Chem. Phys. **95**, 323 (1991).
[13] M. Lucke, M. Mihelcic, and B. Kowalski, Phys. Rev. A **35**, 4001 (1987).
[14] D. G. Aronson and H. F. Weinberger, *Advances in Mathematics* (Academic, New York, 1978), Vol. 30.
[15] F. Zhong and R. Ecke, Chaos **2**, 163 (1992).
[16] A. B. Ezersky, A. Garcimartin, J. Burguete, H. L. Mancini, and C. Perez-Garcia, Phys. Rev. E **47**, 1126 (1993).
[17] P. M. Parmentier, V. C. Regnier, and G. Lebon, J. Heat Mass Transfer **36**, 2417 (1993).
[18] B. S. Martincigh and R. H. Simoyi, Phys. Rev. E **52**, 1606 (1995).
[19] D. A. Vasquez, J. W. Wilder, and B. F. Edwards, Phys. Fluids A **4**, 2410 (1992).
[20] C. R. Chinake and R. H. Simoyi, J. Phys. Chem. **98**, 4012 (1994).
[21] An extreme case are propagating flame fronts, see J. F. Clarke, Prog. Energy Combust. Sci. **15**, 241 (1989).
[22] C. R. Chinake and R. H. Simoyi, Physica D (to be published).
[23] D. Horvath, V. Petrov, S. K. Scott, and K. Showalter, J. Chem. Phys. **89**, 6332 (1993).
[24] I. R. Epstein, K. Kustin, and R. H. Simoyi, J. Phys. Chem. **96**, 5852 (1992).
[25] C. R. Chinake and R. H. Simoyi, J. Phys. Chem. **97**, 11 569 (1993).
[26] C. R. Chinake, E. Mambo, and R. H. Simoyi, J. Phys. Chem. **98**, 2908 (1994).
[27] H. Taube and H. Dodgen, J. Am. Chem. Soc. **71**, 3330 (1949).
[28] Gy. Rabai and M. Orban, J. Phys. Chem. **97**, 5935 (1993).
[29] Barium chloride, $BaCl_2$, reacts with sulfate to produce a white precipitate of $BaSO_4$. Thus the presence of sulfate

and hence the wave front could easily be detected in the white precipitate formation.
[30] R. H. Simoyi and K. J. TerBeek, Chem. Eng. News **71**, 4 (1993).
[31] A. Indelli, J. Phys. Chem. **68**, 3027 (1964).
[32] M. J. B. Hauser and R. H. Simoyi, Phys. Lett. A **191**, 31 (1994).
[33] M. J. B. Hauser and R. H. Simoyi, Chem. Phys. Lett. **227**, 593 (1994).
[34] H. E. Huppert and J. S. Turner, J. Fluid Mech. **106**, 299 (1981).
[35] J. S. Turner, Ann. Rev. Fluid Mech. **17**, 11 (1985).
[36] J. A. Pojman and I. R. Epstein, J. Phys. Chem. **94**, 4966 (1990).
[37] J. A. Pojman, I. R. Epstein, and I. Nagy, J. Phys. Chem. **95**, 1306 (1995).
[38] I. P. Nagy, A. Keresztessy, J. A. Pojman, Gy. Bazsa, and Z. Noszticzius, J. Phys. Chem. **98**, 6030 (1994).
[39] B. F. Edwards, J. W. Wilder, and K. Showalter, Phys. Rev. A **43**, 749 (1991).
[40] Strictly speaking, Eq. (8) will apply only to specific regions as the temperature and specific gravity are not uniform throughout the whole solution.
[41] D. A. Vasquez, J. M. Littley, J. W. Wilder, and B. F. Edwards, Phys. Rev. E **50**, 280 (1994).
[42] M. E. Stern, Tellus **12**, 172 (1960).
[43] D. Villers and J. K. Platten, J. Fluid. Mech. **234**, 487 (1992).
[44] Ming-I Char and Ko-Ta Chiang, J. Phys. D **27**, 748 (1994).
[45] J. A. Szymczyk, Can. J. Chem. Eng. **69**, 1271 (1991).

(a)

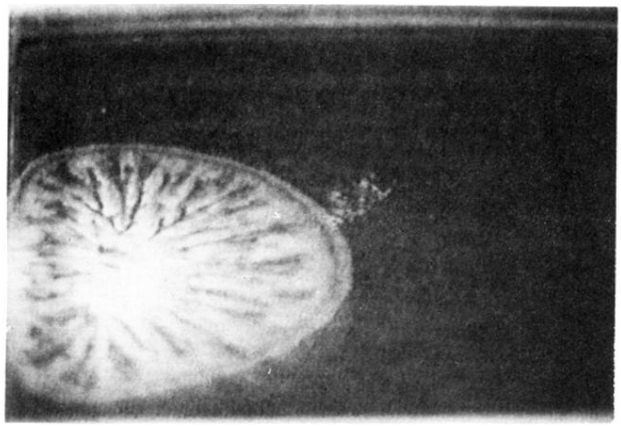

(b)

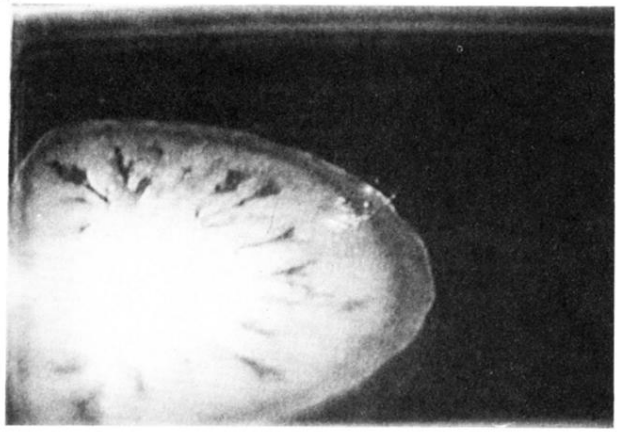

(c)

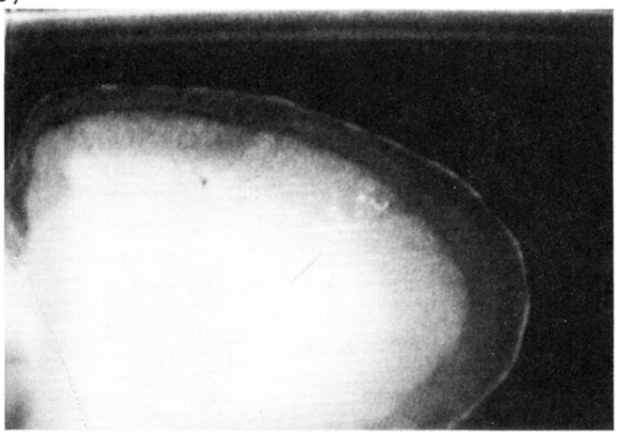

FIG. 2. Structured (or inhomogeneous) precipitation patterns mentioned in Fig. 1. The thin annulus of null precipitation at the edge of the wave front is also quite evident. $[NaClO_2]_0=0.048$ M, $[SC(NH_2)_2]_0=0.024$ M, and $[BaCl_2]_0=0.020$ M. (b) Further development of the wave shown in (a). The inhomogeneous precipitations patterns are beginning to be annihilated, and two regions can now be seen, with the region of faint precipitation at the wave front. (c) Same wave as in (a) and (b) about 5 s after (b). The precipitation patterns have now been destroyed, and three regions can now be seen: faint precipitation (region I), thicker precipitation (region II), and thickest precipitation (region III).

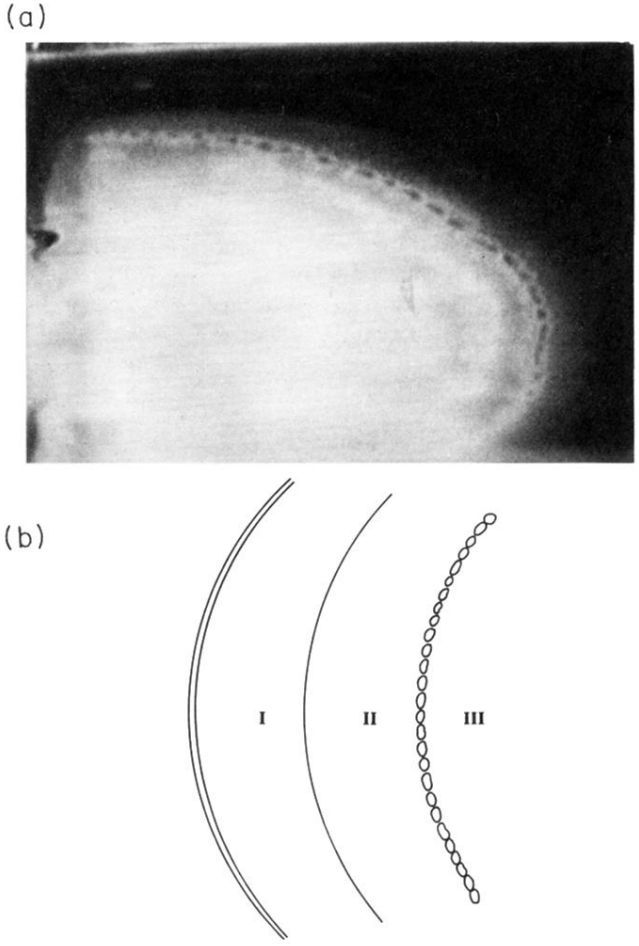

FIG. 3. (a) A picture showing the three regions as well as the thermal plumes at the interface between regions II and III. Experimental conditions are the same as in Fig. 2. (b) A schematic sketch of the picture shown in (a).